Dedicated to innovation in aerospace

NLR-TP-2021-037 | October 2021

Investigation of passive and active drag reduction concepts for the improvement of aerodynamic characteristics of trucks within the AEROFLEX project

CUSTOMER: European Commission

Royal NLR – Netherlands Aerospace Centre

Dedicated to innovation in aerospace

Investigation of passive and active drag reduction concepts for the improvement of aerodynamic characteristics of trucks within the AEROFLEX project

REPORT NUMBER
NLR-TP-2021-037

AUTHOR(S)
O.J. Bartels
J. van Muijden
K.H. Lammers
D. Rentema

REPORT CLASSIFICATION
UNCLASSIFIED

DATE
October 2021

KNOWLEDGE AREA(S)
Computational Physics and Theoretical Aerodynamics
Aeroacoustic and Experimental Aerodynamics

DESCRIPTOR(S)
Truck aerodynamics
Drag reduction
Flow control

Problem area

There is a strong wish for and emphasis on disruptive changes in the transport sector to facilitate the energy transition to greener variants of transportation, fed by international political agreements and national initiatives to improve the quality of life. As the transport sector contributes to about 25% of total CO2-emissions in the EU, there is a strong objective for the reduction of CO2 and NOx emissions in the near future. On the other side, the demand for transportation of goods and passengers is showing a significant increase for decades to come. Creating a cleaner and greener society assumes that major technological steps forward will be accomplished in the coming decade to assure that the near-term and long-term objectives for emissions will be met.

In the framework of the European project “Aerodynamic and Flexible Trucks for Next Generation of Long Distance Road Transport – AEROFLEX”, drag reduction devices using active and passive geometrical and flow control concepts are being investigated to significantly improve the fuel efficiency of long-haul road transportation.

Description of work

This paper focuses on the following topics. First, the Generic European Transport System (GETS) configuration, which is a simplified truck geometry well suited for conceptual studies, is presented on a code-to-code comparison basis using NLR's in house flow solver ENSOLV, STAR-CCM+, and openFOAM. Second, a 2022 entry-into-service tractor-trailer combination was studied using openFOAM, and the impact of several technologies on its aerodynamic drag was investigated: a boattail, extended deflectors, active geometry, tangential blowing, base bleeding and lower base bleeding. Finally, the creation of the wind tunnel model and planning of the test campaign is discussed with the purpose of CFD-validation.

Results and conclusions

The boattail leads to a significant reduction in drag for both the baseline and the GETS configuration. Extending the deflectors to cover the truck-trailer gap leads to reduced drag as well. Although fully extending the deflectors seems most effective, extending them partially across this gap still leads to a reduction in drag. CFD analyses show that tangential blowing combined with a higher slant angle of the boattail top panel does not lead to a reduction in aerodynamic drag. Base bleeding does show a reduction in drag, however, this reduction will have to offset the higher fuel burn required to generate the mass flow needed. Mimicking the fourth boattail panel by blowing air into the wake at a high velocity (lower base bleeding) leads to a change in wake structure and an increase in aerodynamic drag.

To validate the CFD results wind tunnel campaigns have been conducted with a 1:3 scale model manufactured by NLR. The aim of the first wind tunnel entry was to validate CFD computations, while the second entry focused on combinations of the most promising drag reduction concepts.

Applicability

The work performed within AEROFLEX provides insight into aerodynamic drag encountered by trucks and methods to reduce this. Combining CFD analyses and wind tunnel test results provides a solid basis for further developing the identified drag reduction devices into real world applications on heavy duty vehicles.

GENERAL NOTE
This report is based on a presentation held at the COMVEC conference, Indianapolis, September 9-11, 2019.

Royal NLR
Anthony Fokkerweg 2
1059 CM Amsterdam, The Netherlands
p) +31 88 511 3113
e) info@nlr.nl i) www.nlr.nl

Dedicated to innovation in aerospace

NLR-TP-2021-037 | October 2021

Investigation of passive and active drag reduction concepts for the improvement of aerodynamic characteristics of trucks within the AEROFLEX project

CUSTOMER: European Commission

AUTHOR(S):

O.J. Bartels	NLR
J. van Muijden	NLR
K.H. Lammers	NLR
D. Rentema	DAF

Royal NLR – Netherlands Aerospace Centre

This report is based on a presentation held at the COMVEC conference, Indianapolis, September 9-11, 2019.

This publication has been refereed by the "Advisory Committee Knowledge and Technology.

CUSTOMER	**European Commission**
CONTRACT NUMBER	**-----**
OWNER	**NLR**
DIVISION NLR	**Aerospace Vehicles**
DISTRIBUTION	**Unlimited**
CLASSIFICATION OF TITLE	**UNCLASSIFIED**

APPROVED BY:		**Date**
AUTHOR	J. van Muijden	28-10-2021
REVIEWER	B.J.G. Eussen	01-11-2021
MANAGING DEPARTMENT	O.J. Bartels	28-10-2021

Contents

Abbreviations

ACRONYM	DESCRIPTION
AEROFLEX	Aerodynamic and Flexible Trucks for Next Generation of Long Distance Road Transport
CFD	Computational Fluid Dynamics
CFVT	Cross-Flow Vortex Trapping
DNW	German-Dutch Wind Tunnels
EARSM	Explicit Algebraic Reynolds Stress Model
EIS	Entry-into-service
GETS	Generic European Transport System
NLR	Royal Netherlands Aerospace Centre
RANS	Reynolds Averaged Navier-Stokes
SST	Shear Stress Transport

20XX-01-XXXX

Investigation of passive and active drag reduction concepts for the improvement of aerodynamic characteristics of trucks within the AEROFLEX project

Abstract

There is a strong wish for and emphasis on disruptive changes in the transport sector to facilitate the energy transition to greener variants of transportation, fed by international political agreements and national initiatives to improve the quality of lifeAs the transport sector contributes to about 25% of total CO_2-emissions in the EU, there is a strong objective for the reduction of CO_2 and NO_x emissions in the near future. On the other side, the demand for transportation of goods and passengers is showing a significant increase for decades to come. Creating a cleaner and greener society assumes that major technological steps forward will be accomplished in the coming decade to assure that the near-term and long-term objectives for emissions will be met.

In the framework of the European project "Aerodynamic and Flexible Trucks for Next Generation of Long Distance Road Transport – AEROFLEX", drag reduction devices using active and passive geometrical and flow control concepts are being investigated to significantly improve the fuel efficiency of long-haul road transportation. This paper focuses on the following topics. First, the Generic European Transport System (GETS) configuration is presented on a code-to-code comparison basis using NLR's in house flow solver ENSOLV, STAR-CCM+, and openFOAM. Second, a 2022 entry-into-service tractor-trailer combination was studied using openFOAM, and the impact of several technologies on its aerodynamic drag was investigated: extended deflectors, active geometry, tangential blowing, base bleeding and lower base bleeding. Finally, the creation of the wind tunnel model and planning of the test campaign is discussed with the purpose of CFD-validation.

Introduction

International political agreements and national initiatives to improve the quality of life by promoting a cleaner and greener society are increasingly exerting their impact on all means of transportation. As the transport sector contributes to about 25% of total CO_2-emissions in the EU, there is a strong emphasis on the reduction of CO_2 and NO_x emissions in the near future [1]. At the same time, the demand for transportation of goods and passengers is showing a significant increase in all projections for decades to come [2]. In order to actually arrive at a cleaner and greener society, disruptive changes are needed to assure that the near-term and long-term objectives for emissions will be met.

NLR is a partner in the European project "Aerodynamic and Flexible Trucks for Next Generation of Long Distance Road Transport - AEROFLEX" [3]. In this project, active since October 2017 and running for a period of 42 months, the objectives are to develop and demonstrate new technologies, concepts and architectures for complete vehicles that are energy efficient, safe, comfortable, configurable and cost-effective. At the same time, varying needs of customers are satisfied by being flexible and adaptable with respect to continuously changing operational conditions. As part of the innovative technologies involved, the improvement of the economic viability of trucks by minimizing the aerodynamic drag is being investigated using all potentially promising means to influence the flow. Ways to improve the aerodynamic efficiency by the application of both passive and active geometrical and flow control concepts are investigated on their merits using Computational Fluid Dynamics (CFD), with verification and validation foreseen through wind tunnel testing and road demonstrator trials. The project aims to establish a 5-10 percent improved energy efficiency through aerodynamic drag reduction using a smart selection of promising drag reducing concepts [4].

This paper is divided into the following sections:

1. Simplified configuration: the results of the code-to-code comparison are presented in this section
2. Baseline truck configuration calculations with and without selected concepts for aerodynamic drag reduction
3. Way forward towards verification and validation of results.

In the following, a description of these aspects is given.

Simplified configuration analysis

For flow solver assessment and comparison purposes, use is made of a simplified geometry known as the Generic European Transport System (GETS). It is a straightforward box-like shape with rounded edges at the front. Its definition and earlier use is described in [5] [6]. The geometry of the baseline GETS is shown in Figure 1 (top). The distance between lower side of the vehicle and the road is 0.49 m. A view from the rear in Figure 1 (middle) shows the blunt trailer end with colored faces which have been used for base bleed and base suction boundary conditions prescription. As a more advanced elaboration of this simple geometry, i.e. a version including a boat tail at the trailer end, has been generated as well, see Figure 1 (bottom). On the inner side of the boat tail, once again surfaces have been defined for base bleed flow conditions. As this geometry is so simple, it is a perfect test case for code-to-code comparisons, grid refinement studies, and evaluation of the effectiveness of flow control concepts.

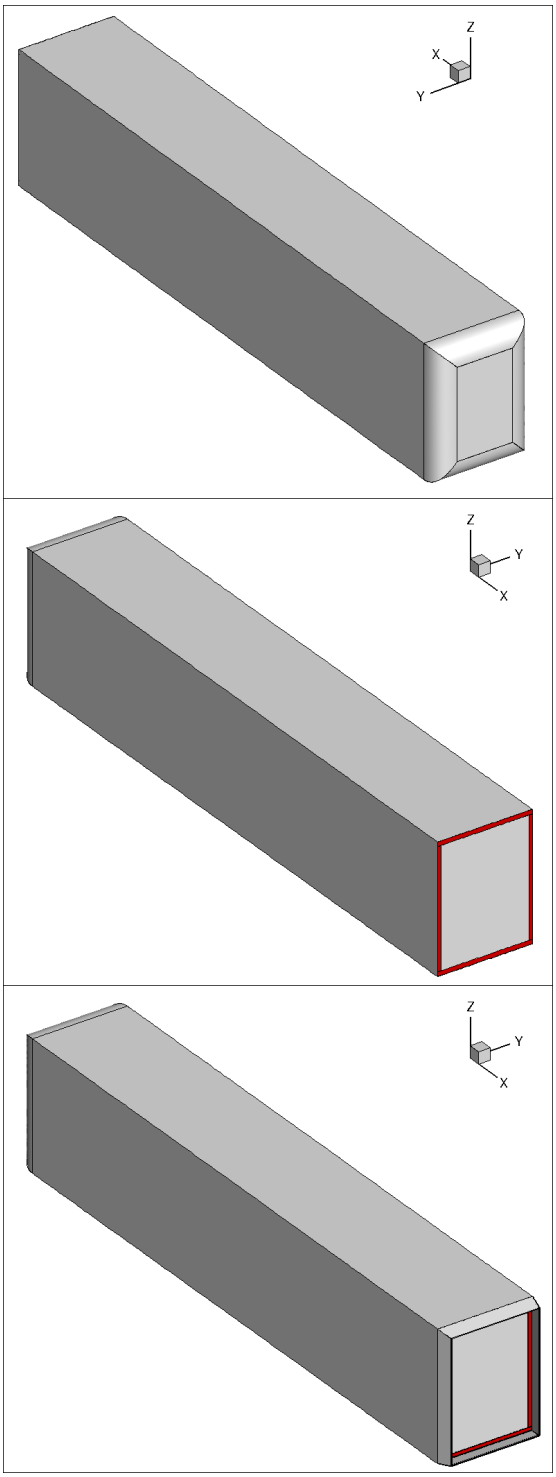

The multi-block structured meshes created for these two variants of the GETS configuration contain 4 grid levels of refinement with a number of cells ranging from about 80,000 cells to about 47 million cells. Each next finer level of the mesh contains exactly 8 times the number of cells on the previous level due to doubling of the cells in each space direction. The precise number of grid cells are given in Table 1.

Table 1: Mesh densities on different levels of the multi-block structured meshes of the GETS variants – total number of cells

Configuration	Coarse	Medium	Fine	Extra fine
Baseline GETS	81,728	653,824	5,230,592	41,844,736
GETS with boat tail	91,264	730,112	5,840,896	46,727,168

Computational methods

Three different, available methods have been used for the code-to-code comparison effort.

The NLR in-house developed flow solver suite ENFLOW contains tools for multi-block topology generation, structured meshing, and viscous flow analysis on the basis of the full Navier-Stokes equations for compressible flow. It employs a finite-volume discretization of the time-dependent compressible mass, momentum and energy equations. For incompressible flows at low speeds as for the current applications, having Mach numbers below 0.1, preconditioning is used to achieve faster convergence of coefficients and flow residuals. Multi-grid acceleration is used whenever possible to improve the convergence speed of the flow solution on the finer meshes. To resolve turbulent stresses, use is made of the k-ω TNT turbulence model enhanced with an Explicit Algebraic Reynolds Stress Model (EARSM). The moving road is included in the simulations by a boundary condition that prescribes a velocity on the solid wall in x-direction, i.e. opposite to the driving direction. Inflow conditions of the air are automatically handled on the basis of prescribed side slip angle. In the current simulations, no use is made of atmospheric boundary layer inflow conditions, as this is usually neglected by truck manufacturers during the design phase.

The commercial solver STAR CCM+ is a solver by Siemens [7]. It contains tools for meshing, flow analysis and post processing. For the mesh a trimmed unstructured hex mesh is used with prism layers around the GETS to account for boundary layers (which are solved using wall-functions). The mesh around the GETS is refined using increasingly small boxes where the mesh size decreases by a factor 2 in each box. For the calculations the Reynolds Averaged Navier-Stokes equations are used with the realizable k-epsilon two-layer turbulence model.

The open source flow solver simpleFOAM from the openFOAM software [8] is used in combination with its snappyHexMesh utility to create the mesh. snappyHexMesh creates a hex-based unstructured grid. Refinement regions are used to control the mesh resolution near the truck and in the wake, and a prismatic layer is applied to all surfaces of the GETS geometry. simpleFOAM solves the Reynolds-averaged Navier-Stokes (RANS) equations, and the *k-ω* Shear Stress Transport (SST) turbulence model [9] is used to resolve the turbulent

stresses. Wall functions are applied to model the velocity in the boundary layer. A moving wall boundary condition is applied to the lower boundary of the domain to simulate the moving road.

For the computations using unstructured CFD-methods, separate meshes have been generated using the mesh generator of each package. For STAR CCM+, the baseline GETS configuration is meshed using 11.95 million cells and cell halving resulted in a finer mesh of 74.11 million cells. For openFOAM, the mesh contains 19 million cells.

Results of code-to-code comparison

For the baseline GETS configuration, a code-to-code comparison has been performed at a wind speed of 25 m/s at three different yaw angles, 0, 5, and 10 degrees yaw. For all these conditions, steady flow simulations have been performed. A solution was said to be converged when the variation in force coefficients were smaller than a count.

In Figure 2, a comparison is shown of the symmetry plane solutions of the velocity in x-direction for the baseline GETS configuration (i.e. no active or passive flow control) at zero side slip, showing from top to bottom the results obtained with ENFLOW, STAR CCM+, and openFOAM. It is found that the flow fields at the front of the vehicle compare very well. Differences can be observed at the rear end of the configuration, in the near wake region. It can be seen that the wake resulting from the ENFLOW simulation appears to have less deeply negative velocities in x-direction in the recirculating zone in the wake. The region with negative velocities is slightly different in size and in shape in each flow solution, details that can probably be attributed to turbulence models used, the mesh resolution as applied in the wake, and flow solver specific characteristics such as the spatial discretization that was used.

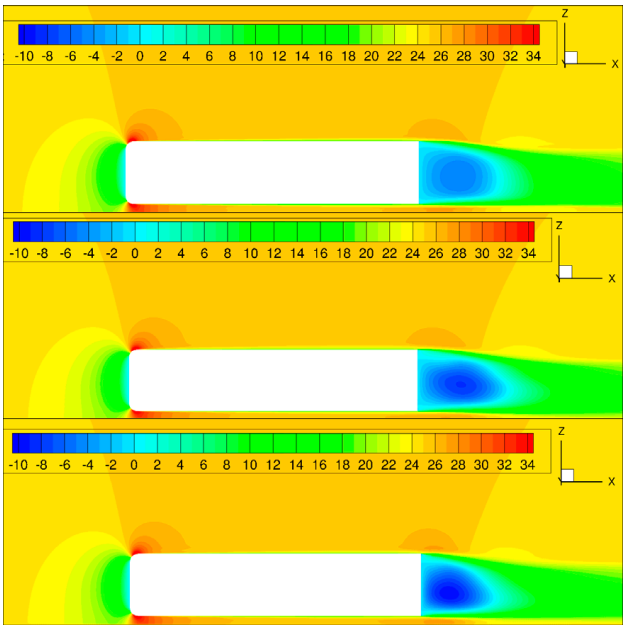

Figure 2: Sideview, code-to-code comparison of symmetry plane solutions of velocity in x-direction for baseline GETS at zero yaw. From top to bottom: ENFLOW, STAR CCM+, openFOAM

For a plane at half vehicle height (Z=2.2475 m), a horizontal cross section is made to look at the flow fields from a different perspective. Figure 3 shows a top view comparison of solutions in this plane. Once again, the flow fields at the front side of the vehicle show very similar characteristics. In the wake, differences appear in shape and size of the region with negative velocities in x-direction. The extent and the shape of the recirculating wake region differ a little, with possible causes as identified above.

Since the flow fields are not in all respects identical, it is interesting to assess how this fact is reflected in the drag coefficient. A direct comparison of baseline GETS drag data at zero side slip using three different flow solvers is shown in Figure 4, where the drag data are plotted against the relative mesh size h. In order to be able to include the unstructured mesh results as well, for these baseline GETS meshes $h=174/(\#cells)^{1/3}$ is used. Despite significant differences in computational schemes and types of meshes and the demonstrated large mesh dependency of drag data, the finest mesh results of all flow solvers more or less show convergence to a common value within a certain scatter band.

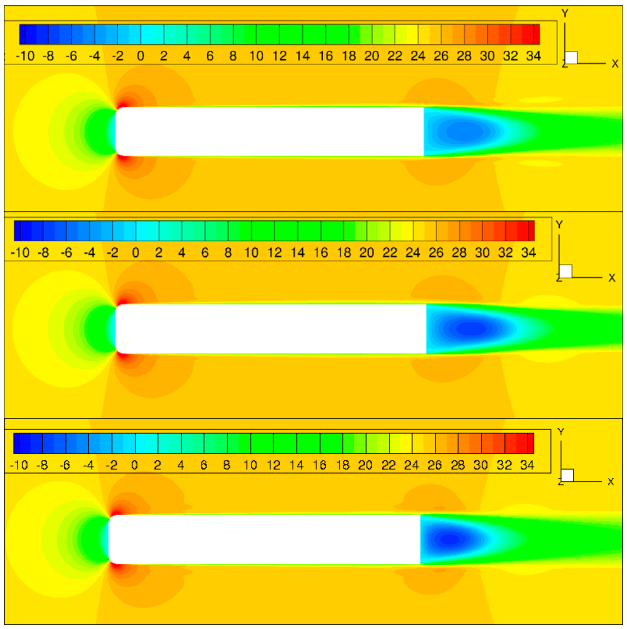

Figure 3: Top view, code-to-code comparison of velocity in x-direction in a cutting plane at half vehicle height at zero yaw. From top to bottom: ENFLOW, STAR CCM+, openFOAM

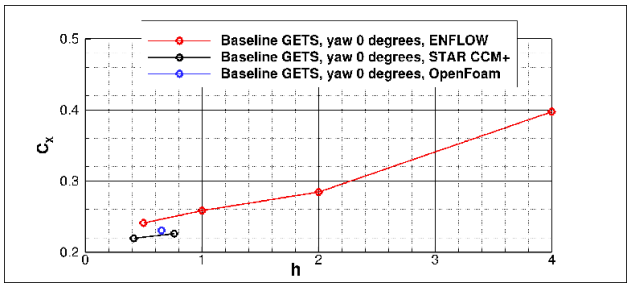

Figure 4: Drag data plotted against the relative mesh size h at zero yaw, showing the dependency of computed drag data as a function of the mesh density

A similar comparison is made for the case with side slip angle of 5 degrees. The symmetry plane solutions are depicted in Figure 5 and the associated flow fields at half vehicle height are given in Figure 6. Now, the symmetry plane solutions in Figure 5 still show a large resemblance to each other with a somewhat shorter region of negative velocities in x-direction as compared to the zero yaw case, but Figure 6 shows a significant difference in contraction of the wake at some distance downstream from the vehicles trailing edge. Before attempting to draw any conclusions from this finding, let us take a look at the associated drag coefficients and also at the comparisons at larger side slip angle. The comparison of aerodynamic coefficients in x-direction for the 5 degrees yaw case is shown in Figure 9. Most flow solvers show an increase in Cx – compared to the zero yaw case – of approximately 0.02. openFOAM shows the smallest increase with yaw angle, however, and is not in line with the other two flow solvers.

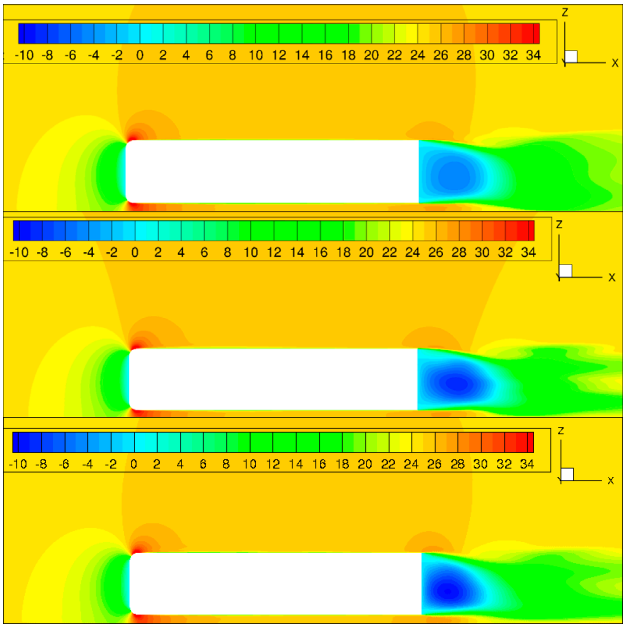

Figure 5: Side view, code-to-code comparison of symmetry plane solutions of velocity in x-direction for baseline GETS at 5 degrees yaw. From top to bottom: ENFLOW, STAR CCM+, openFOAM

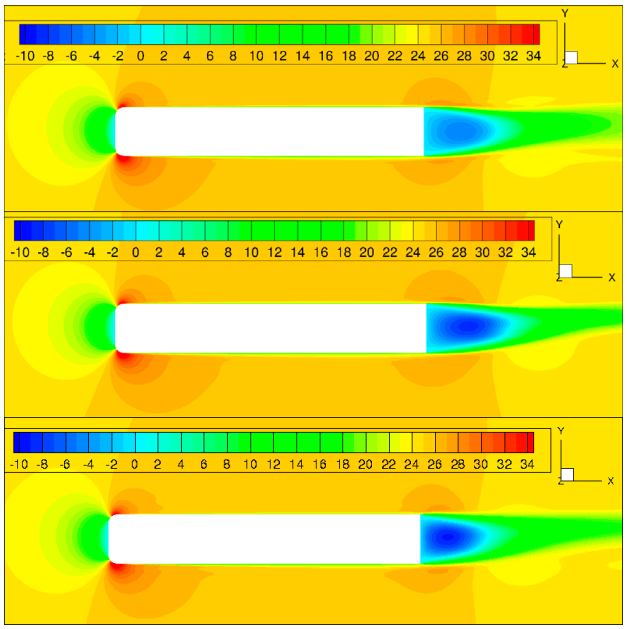

Figure 6: Side view, code-to-code comparison of velocity in x-direction in a cutting plane at half vehicle height at 5 degrees yaw. From top to bottom: ENFLOW, STAR CCM+, openFOAM

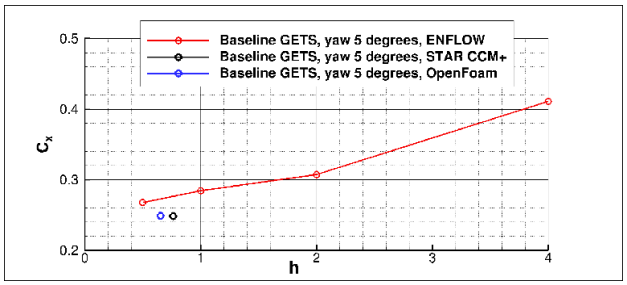

Figure 7: C_x-data plotted against the relative mesh size h for 5 degrees yaw

For 10 degrees side slip, the same comparative pictures are shown in Figure 8, 9, and 10. The symmetry plane flow solutions shown in Figure 7 depict a decrease in the length of the region with negative flow velocities as compared to those for 5 degrees side slip, a finding which is confirmed by the results shown in Figure 8. Here, too, the contraction in the wake of the flow solutions is somewhat different between flow solvers and could possibly be related to turbulence mixing properties of the used turbulence models. Most striking is the unexpected flow separation at the rounded leading edge in the openFOAM results. In Figure 12, the aerodynamic coefficient in x-direction is shown. The openFOAM force coefficient in x-direction, however, now show an excessive increase compared to the other flow solvers that show a more regular increase in C_x, in accordance with expectations. The reason for this behaviour is the separation occurring at the rounded leading edge.

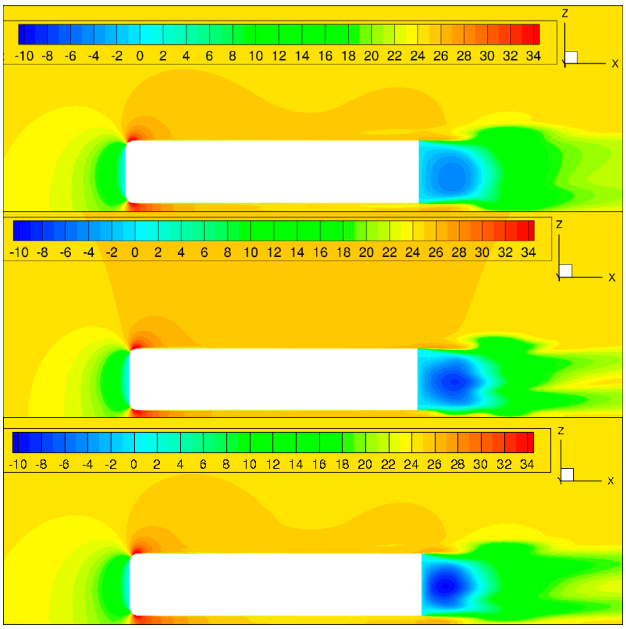

Figure 8: Code-to-code comparison of symmetry plane solutions of velocity in x-direction for baseline GETS at 10 degrees yaw. From top to bottom: ENFLOW, STAR CCM+, openFOAM

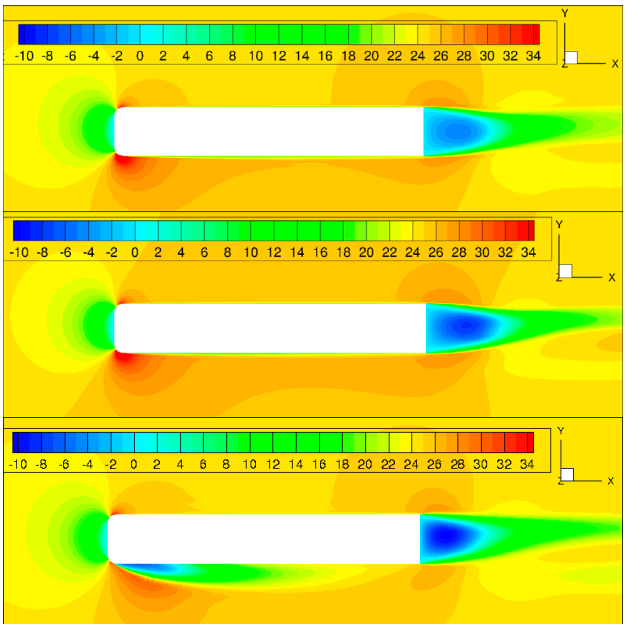

Figure 9: Code-to-code comparison of velocity in x-direction in a cutting plane at half vehicle height at 10 degrees yaw. From top to bottom: ENFLOW, STAR CCM+, openFOAM

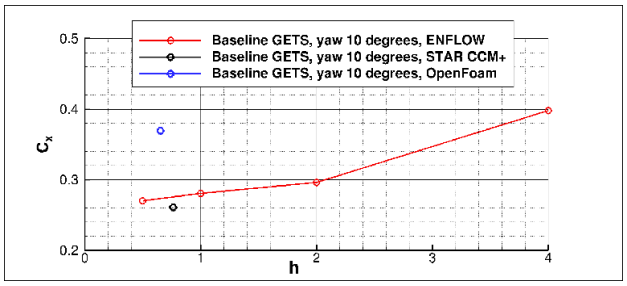

Figure 10: C_x-data plotted against relative mesh size h for 10 degrees yaw

Flow control concepts applied to GETS

Apart from analysis of the baseline GETS configuration to obtain a reference starting point and performing code-to-code comparisons, several flow control concepts have been applied to the GETS in order to assess their impact on the drag of the configuration and their potential for real life applications. The concepts applied to the GETS configuration that are reported here consist of base suction, base bleed, boat tail, and a combination of boat tail and base bleed. The amount of base bleed and base suction has been varied in several simulations, results shown below in the cutting planes employ a total mass flux of 3.7 kg/s.

Results of flow control concepts

The impact of flow control concepts on the flow field in the symmetry plane of the GETS are shown in Figure 11 and the associated pictures in a horizontal cutting plane at half vehicle height are shown in Figure 12.

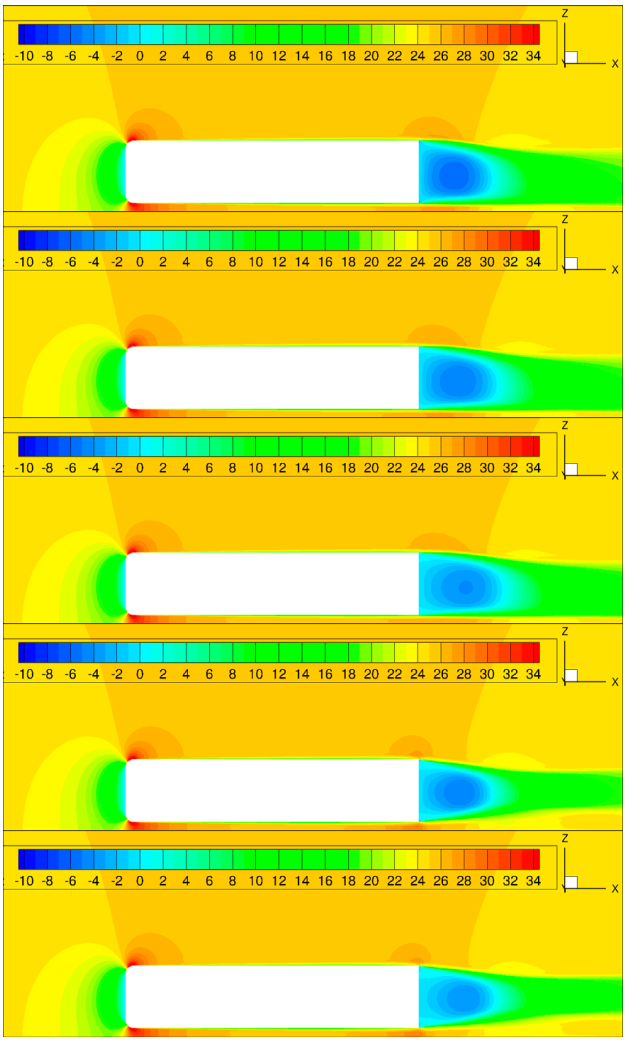

Figure 11: Side view, impact of flow control concepts on the flow field in the symmetry plane at zero yaw (ENFLOW results). From top to bottom: base suction, baseline GETS, base bleed, boat tail, boat tail with base bleed

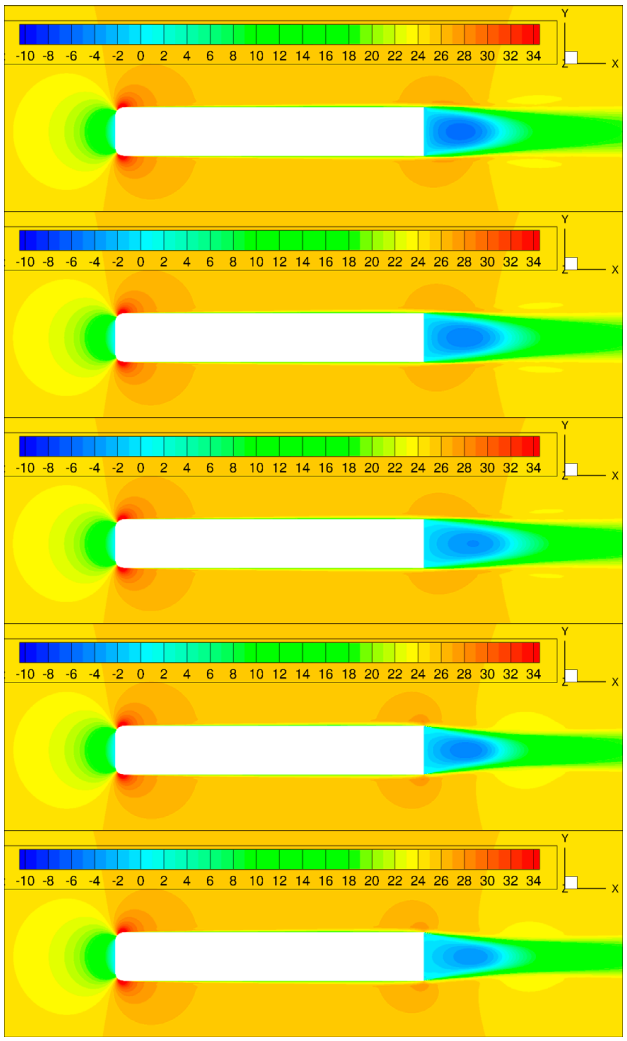

Figure 12: Top view, impact of flow control concepts on the flow field in the cutting plane at half vehicle height (ENFLOW results) at zero yaw. From top to bottom: base suction, baseline GETS, base bleed, boat tail, boat tail with base bleed

Base suction employs a prescribed mass flux ratio in the negative x-direction, i.e. out of the flow domain, whereas base bleed employs a prescribed mass flux ratio in the positive x-direction, into the flow domain. The direct visible result of base suction is a somewhat local indentation of the region of negative velocities in x-direction and a somewhat shorter near wake region. It seems that base bleed reduces the negative velocities in the near wake and results in the largest recirculating zone. The boat tail has a significant impact on the reduction of the size of the recirculating zone in the near wake and the width of the wake further downstream. The boat tail with base bleed (blowing velocities applied at the inside of the boat tail, blowing direction in x-direction) extends the recirculating zone a little, while at the same time the base bleed once again reduces the absolute magnitude of the negative velocities in the recirculating zone.

How the flow control concepts influence the drag data is shown in the following. The mesh dependency of drag data (more precisely, the force coefficient in x-direction, Cx) of the GETS configuration with several flow control concepts is shown in Figure 13. All simulated results show a consistent drag decrease with denser meshes (smaller relative mesh size). Furthermore, the mesh dependency is quite significant, and even on the extra fine meshes applied there is no reason to expect that the drag values are close to the final mesh-converged values. Therefore, the need for a good and meticulously performed experiment is still of use for establishing the reference values.

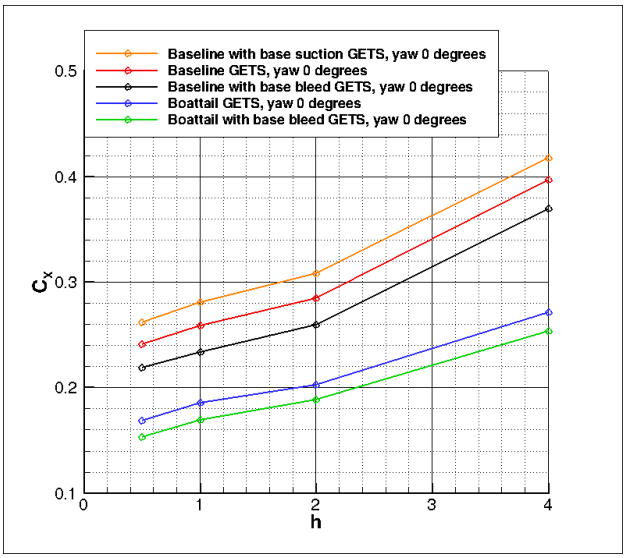

Figure 13: Mesh dependency of drag data for GETS with multiple flow control concepts at zero yaw angle, ENFLOW results

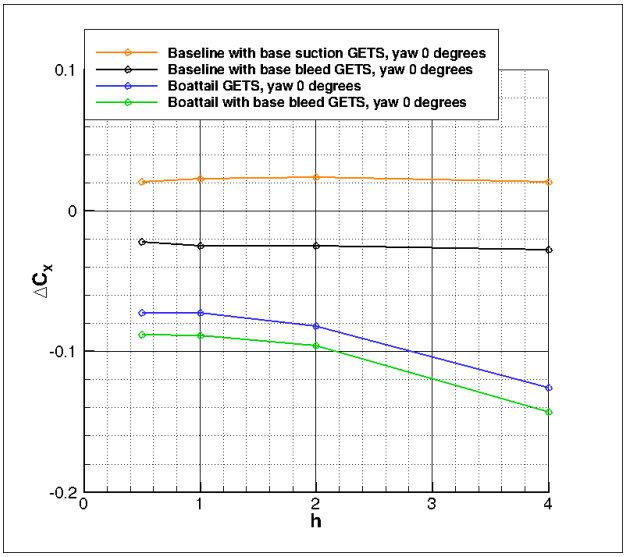

Figure 14: Mesh dependency of drag differences due to several flow control concepts at zero yaw angle, ENFLOW results

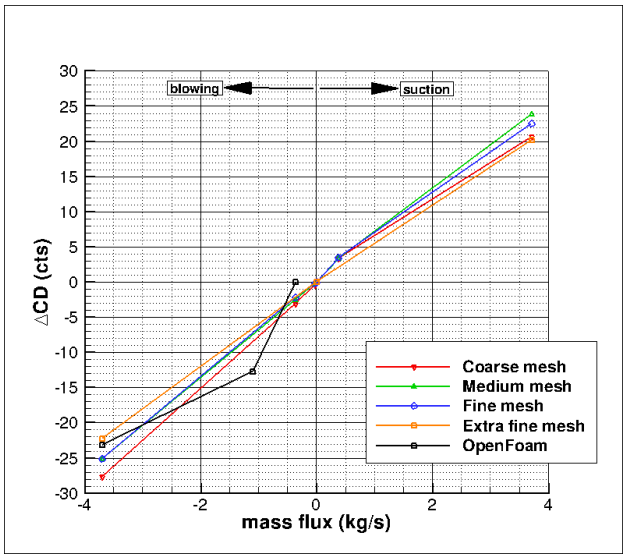

Figure 15: Compiled results for the impact of suction and blowing at the base of the GETS on drag at zero yaw angle: ENFLOW results versus openFOAM

Table 2: Impact of flow control concepts on Cx, computed at the finest mesh resolution (h = 0.5). Cx values are in counts (percentage)

	Angle of sideslip		
Case	**0**	**-5**	**-10**
GETS baseline	241.1	267.3	270.2
ΔCx, base bleed, 3.7 kg/s	-22.3 (-9%)	-23.7 (-9%)	-24.3 (-9%)
ΔCx, boattail	-72.9 (-30%)	-71.7 (-27%)	-67.5 (-25%)
ΔCx, boattail + base bleed, 3.7 kg/s	-88.0 (-37%)	-88.7 (-33%)	-86.0 (-32%)

Taking the baseline configuration drag data as a reference, Figure 14 and Table 2 show the drag differences with the baseline due to several flow control concepts. It is shown that the delta-Cx values converge more rapidly with mesh resolution than the directly calculated drag data. Thus, the drag improvements due to flow control concepts can be assessed on a much more relaxed mesh density. Similar results have been found for the mesh-dependent results for 5 and 10 degrees yaw angle. Both the boattail and the base bleeding result in a reduction in aerodynamic drag in this configuration, and the impact of base bleeding combined with a boattail is smaller than the impact of base bleeding without a boattail present.

Compiled results for base bleed and base suction versus mass flux at zero yaw angle are shown in Figure 17, comparing the results of two different flow solvers. It seems that base suction has no beneficial impact on drag, whereas base bleed can provide significant additional drag benefits.

Baseline geometry analysis

In this section the analysis of the AEROFLEX baseline geometry using openFOAM is presented. The baseline geometry represents a 2022 entry-into-service (EIS) truck-trailer combination. It includes trailer side skirts covering the wheels and a boat-tail attached to the base of the trailer. Anticipating a future change in European regulations, the front has been extended by 500 mm, enabling a more aerodynamically shaped truck. Figure 16 (top) gives an impression of the baseline geometry.

This section includes the grid generation process and the applied boundary conditions. Furthermore, the implementation of several drag reduction concepts on the baseline geometry is discussed, and their impact on Cx is presented.

Method

Grid generation is done using openFOAM's snappyHexMesh utility. The computational domain is approximately 20 truck lengths long, 10 truck widths wide and 5 truck heights high. Refinement regions are used to control the resolution of the grid nearer to the truck and in the wake region. A prismatic layer consisting of eight cells with an expansion ratio of 1.2 is applied to selected aerodynamic surfaces, see Figure 16 (bottom) for an overview of the selected surfaces. Applying a prismatic layer to these surfaces only leads to a significant reduction in mesh complexity, as the geometry contains internal surfaces and narrow gaps where generating a grid including a prismatic layer can be problematic. Moreover, the aim of the current study is to investigate the impact of drag reduction concepts. Thus, capturing the trends in drag values is more important than getting an accurate absolute value for the drag for a specific case. The mesh used for the CFD analyses described below consists of approximately 180 million cells.

openFOAM's simpleFoam solver is used in combination with a *k-ω* shear stress transport (SST) [9] turbulence model. Simulations of the baseline geometry are performed with a freestream velocity magnitude of 25 m/s at 0, -5, and -10 degrees of sideslip. The ground plane is prescribed a velocity of 25 m/s in the x-direction, as this represents the driving direction of the truck-trailer combination. The wheels and their connecting axles are prescribed rotating velocities such that the radial velocity of the tires matches the (linear) velocity of the truck, i.e. 25 m/s. The radiator package in front of the engine is modeled as a porous medium, where the Darcy-Forchheimer law [10] is used to model the drop in pressure over the radiator, see equation 1.

$$\Delta p = -\left(\mu d + {}^{1}/_{2}\,\rho \|\boldsymbol{U}\| f\right)\boldsymbol{U} \tag{1}$$

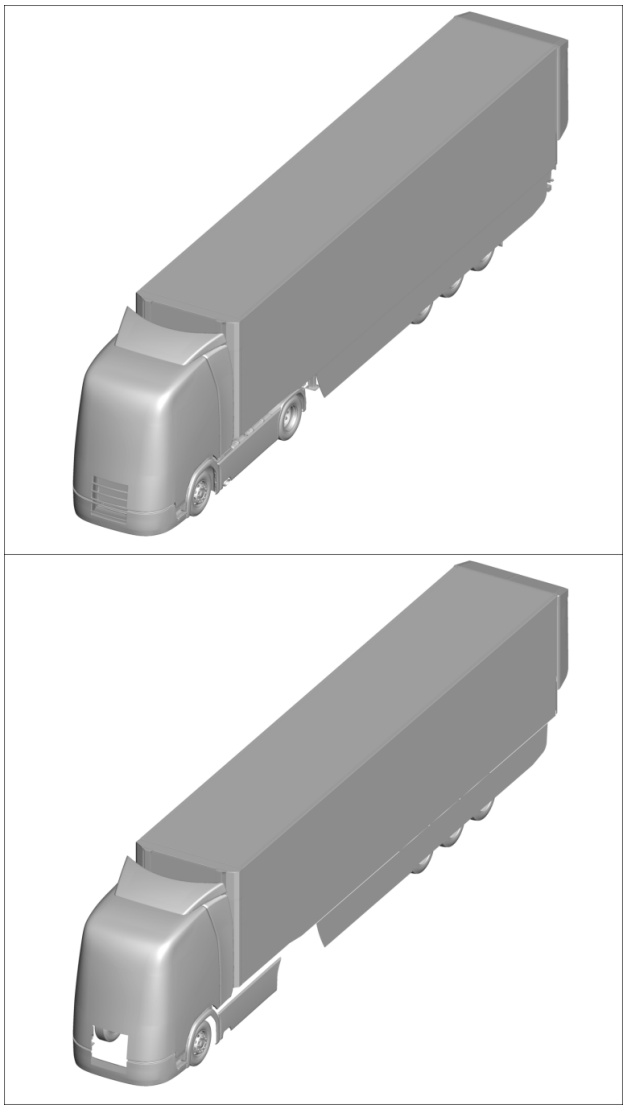

Figure 16: Baseline geometry (top), surfaces selected for prismatic layer during mesh generation (bottom)

Results

First, the results of the baseline geometry simulations are presented. Second, the results of the selected drag reduction concepts will be shown and discussed.

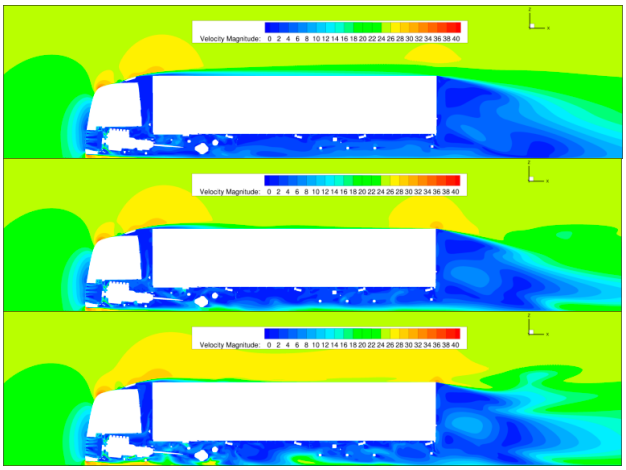

Figure 17: Velocity magnitude in the symmetry plane for three different angles of sideslip, top: 0 degrees, middle: -5 degrees, bottom: -10 degrees

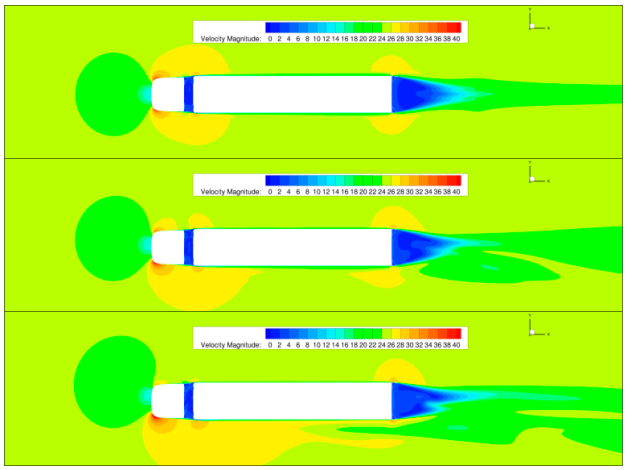

Figure 18: Velocity magnitude in the xy-plane at half the trailer height at different angles of sideslip, top: 0 degrees, middle: -5 degrees, bottom: -10 degrees

The velocity field in the symmetry plane (y = 0.0) and in the xy-plane at half the height of the truck are shown in Figure 17 and Figure 18. It can clearly be seen that the flow accelerates on the top and leeward side of the truck, creating suction peaks there. Furthermore, the flow appears to impinge on the leading edges of the trailer behind the truck, suggesting that a smoother transition from truck to trailer could reduce drag.

The results of the CFD analysis of the baseline geometry are compared with the same geometry excluding the boattail. It is clear that the boattail has a positive impact on the drag of the truck, reducing drag by approximately 10% for all angles of sideslip. To verify that the impact of the boattail is adequately captured these results are compared with results from literature, see Table 3. Boattails have been studied extensively, and reported drag reductions vary depending on the geometry, but most studies show a reduction in drag is achieved by applying a boattail [6] [11] [12] [13]. The reported reductions in drag seem to be higher than the 10% reported here.

Table 3: Impact of boattail on Cx

	Cx **Sideslip angle**		
Case description	0	-5	-10
AEROFLEX baseline without boattail	336	401	472
AEROFLEX baseline	302	359	429
ΔCx	-34 (-10.0%)	-42 (-10.4%)	-43 (-9.2%)
ΔCx, Van Raemdonck, wind tunnel [6]	-12%	-12%	-14%
ΔCx, Hakansson and Lenngren [12] (counts)	-38	-54	-
ΔCx, GETS boattail	-72.9 (-30%)	-71.7 (-27%)	-67.5 (-25%)

Drag reduction concepts

Several drag reduction concepts have been selected for the current studies. These can be divided into the following categories: passive geometry, active geometry, and active flow control.

Extended deflectors

Various studies on reducing drag by modifying the truck-trailer gap have been performed [14]. Wind tunnel experiments have shown that extending the cabin air deflectors can reduce wind-averaged drag by ~8% relative to shorter air deflectors (~25% relative to a configuration without air deflectors) [15]. A CFD investigation into sealing the gap showed a reduction in the wind-averaged drag coefficient of 33 counts, and a gap fairing reduced the drag coefficient by 15 counts [12]. Combining tractor bleed (injecting low velocity air into the truck-trailer gap) with side extenders has been

shown to reduce the drag coefficient by up to 0.146 [16]. Another study into extending roof and side deflectors showed a drag reduction of up to 27% at a high yaw angle [17]. Cross-flow vortex trapping (CFVT) devices were designed and investigated numerically and experimentally, and showed a reduction in fuel consumption 3% to 8% in road tests [18].

For the extended deflectors, the baseline geometry is modified such that the side and roof air deflectors on the tractor are extended rearwards to close the gap between the tractor and the trailer. This should prevent air from flowing into this gap and thus ensure a smoother airflow. The extension is done in two steps: an extension equal to half the length of the gap, partially closing it, and an extension such that the gap is closed entirely, see also Figure 19.

The simulations show that both the half and the full extension of the side and roof air deflectors significantly reduce aerodynamic drag, see also Figure 20 and Table 5. The highest drag reduction is achieved by fully closing the gap between the truck and the trailer. This will generally ensure a smoother flow along the vehicle: in an ideally shaped case there is no impingement on the trailer leading edges and thus no stagnation there, no air flowing into the gap, and no disturbances of the flow on the leeward side of the truck (in case of sideslip).

The results show a drag reduction of 2% to 4% for the half extended deflectors, and a reduction of 4% to 6% for the fully extended deflectors. The observed reduction in drag can be improved further by optimizing the shape of the air deflectors. For the current study these were simply extended rearward in a straight line. This causes a kink in their shape, leading to suction peaks. Smoothly curved surfaces would prevent this and could potentially reduce drag further. The drag reduction seems smallest at an angle of sideslip of -5 degrees.

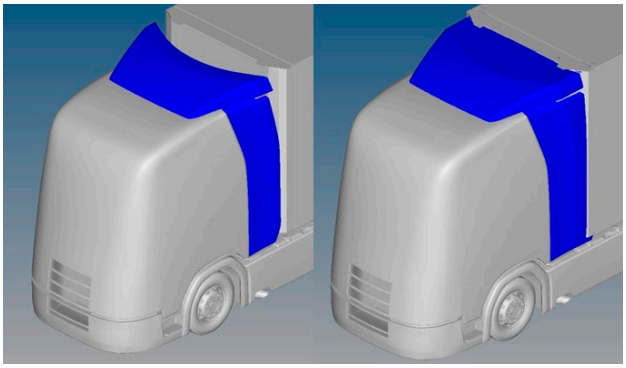

Figure 19: Deflector extension, (l) half extended, (r) fully extended

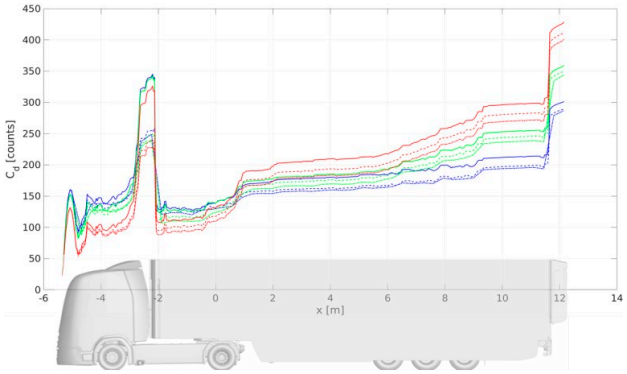

Figure 20: Drag development in x-direction for the extended deflectors compared to the baseline geometry at 0 (blue), -5 (green) and -10 (red) degrees of sideslip. (solid: baseline geometry, dashed: half extension, dotted: full extension)

Active geometry

Active geometry is applied as an asymmetric rotation of the side air deflectors on the tractor, which is rotated outward by 5 degrees. The idea behind this technology is that by rotating the air deflector on the windward side, air is guided past the tractor-trailer gap which moves or removes the stagnation points at the front of the trailer and prevents air from flowing into the gap between the truck and the trailer. This is particularly relevant at higher angles of sideslip, since more air flows into the gap between the tractor and trailer in these cases. For this reason only the cases at -5 degrees and -10 degrees angle of sideslip were analyzed.

At -5 degrees angle of sideslip the rotation has an adverse effect on drag, which increases by approximately 1%. This can be explained by the higher pressure on the rotated deflector. At -10 degrees angle of sideslip, the drag is reduced by approximately 3%. The cause of this drag reduction differs from the extended deflectors, as can be seen in Figure 21.

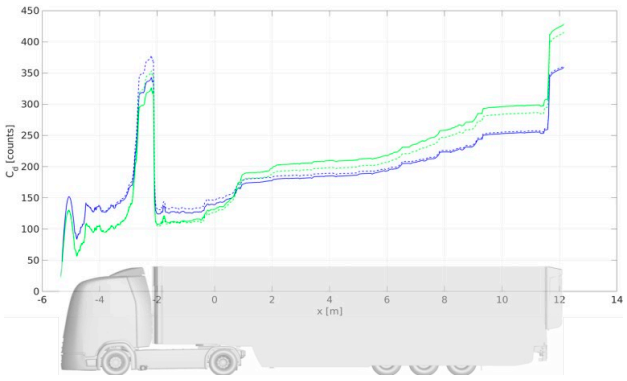

Figure 21: Drag development in x-direction for the active geometry case compared to the baseline geometry at -5 (blue) and -10 (green) degrees of sideslip. (solid: baseline geometry, dashed: active deflector)

Compared to the baseline, the drag development across the truck-trailer gap is equal or higher for the active geometry case at both -5 and -10 degrees of sideslip. However, in the -10 degrees sideslip

case, the drag climbs less rapidly with the rotated air deflector than for the baseline geometry. This indicates that the rotated air deflector interacts with the complex air flow near the rear axle of the truck and the flow underneath the trailer.

Active flow control

Active flow control entails any mechanism that actively influences the local flow in an attempt to reduce aerodynamic drag. Tangential blowing has been shown in the wind tunnel to reduce drag by up to 15% by preventing flow separation and improving pressure recovery on the trailer base [19]. In another study, Coanda blowing showed a fuel burn reduction of ~4% [20]. Tangential blowing in combination with rounded aft trailer edges was shown to reduce drag significantly, leading to potential reduction in power required to overcome aerodynamic and rolling drag of 24% to 32% [21] [22]. Synthetic jets combined with base flaps were studied numerically and experimentally and showed a decrease in drag of 3.1% compared to a geometry without base flaps [23]. Suction and pulsed blowing applied on the trailing edge of a simplified truck geometry were investigated in a wind tunnel and shown to have a drag reduction potential of 20% [24]. Active flow control applied to a generic truck cabin showed a drag reduction of up to 50% depending on the actuation frequency [25]. A different form of active flow control is base bleeding, where air is 'bled' from a rearward facing surface into the wake. Tractor base-bleeding was investigated and shown to reduce drag significantly for a tractor-trailer combination [16]. Base bleeding was shown to reduce the aerodynamic drag of a generic SUV by 0.1 counts [26] and 0.3% to 1.1% [27]. As described above, base bleeding at a mass flow rate of 3.7 kg/s led to a reduction in drag of approximately 6% when combined with a boattail.

In this study, active flow control entails the following technologies: continuous tangential blowing combined with a planar boat tail, base bleeding, and lower base bleeding. The first, tangential blowing, is combined with a higher slant angle of the top panel of the boattail than is applied in the baseline geometry. This higher angle has the potential to reduce drag more than the original boattail by reducing the wake size and improving the pressure recovery on the trailer base, on the condition that the flow over this top panel remains attached. Injecting momentum into the flow by tangential blowing can prevent the flow from separating, keeping it attached to the boattail top panel. Two top panel angles and two tangential blowing velocities are investigated at 0 and -5 degrees angle of sideslip: 16 and 20 degrees and 25 and 60 m/s, respectively.

The velocity magnitude in the symmetry plane for modified boattail geometry is shown without tangential blowing, with blowing at 60 m/s, and at 25 m/s in Figure 22. At a slant angle of 20 degrees, the flow over the top panel of the boattail separates, no longer following the boattail panel. Tangential blowing at 60 m/s causes the flow to reattach, which in turn leads to a smaller wake behind the trailer and an increased pressure recovery on the trailer base, see Figure 23. A tangential blowing velocity of 25 m/s also causes the flow to remain attached to the top panel, although at the panel trailing edge separation does appear to occur. The effect on the wake and trailer base pressure in this case is significantly smaller than in the previous case, however.

Despite the reduction in the wake size and improvement in the pressure recovery on the trailer base, the drag compared to the baseline geometry is roughly the same. The increased angle on the boattail top panel actually increases drag, as the force vector resulting from the negative pressure on the panel is tilted further backwards. This offsets the drag reduction caused by the higher pressure on the trailer base. Thus, the net effect on the drag of the increased top panel slant angle combined with tangential blowing is zero for the 60 m/s case. The net effect of tangential blowing at 25 m/s is barely noticeable and falls within the noise of the analysis.

At a slant angle of 16 degrees, the flow is weakly separated. Tangential blowing at 25 m/s showed reattached flow, with a very small effect on the trailer base pressure. The effect of tangential blowing compared to only increasing the slant angle is shown in Table 4. When compared against the baseline geometry, the simulations show an increase in drag of 1% to 3% in the case of a 20 degree slant angle. In the case of a 16 degree slant angle, the drag is reduced by 1% in the absence of sideslip, and increased by 1% at a sideslip angle of -5 degrees.

Table 4: Contributions to Cx from the trailer base and the boattail top panel for the three cases at 0 degrees sideslip. The combined effects cancel out or are very small. Cx values are reported in counts. Note that the changes are relative to the geometry with the top panel rotated, instead of relative to the baseline geometry

	Slant angle	Cx	ΔCx
Trailer base, Vj = 0 [m/s] **Top panel, Vj = 0 [m/s]**	20	68.6 5.2	- -
Trailer base, Vj = 60 [m/s] **Top panel, Vj = 60 [m/s]**	20	61.5 11.7	-7.1 +6.5
Trailer base, Vj = 25 [m/s] **Top panel, Vj = 25 [m/s]**	20	69.1 6.0	+0.5 +0.8
Trailer base, Vj = 0 [m/s] **Top panel, Vj = 0 [m/s]**	16	65.1 5.6	- -
Trailer base, Vj = 25 [m/s] **Top panel, Vj = 25 [m/s]**	16	64.6 6.5	-0.5 +0.9

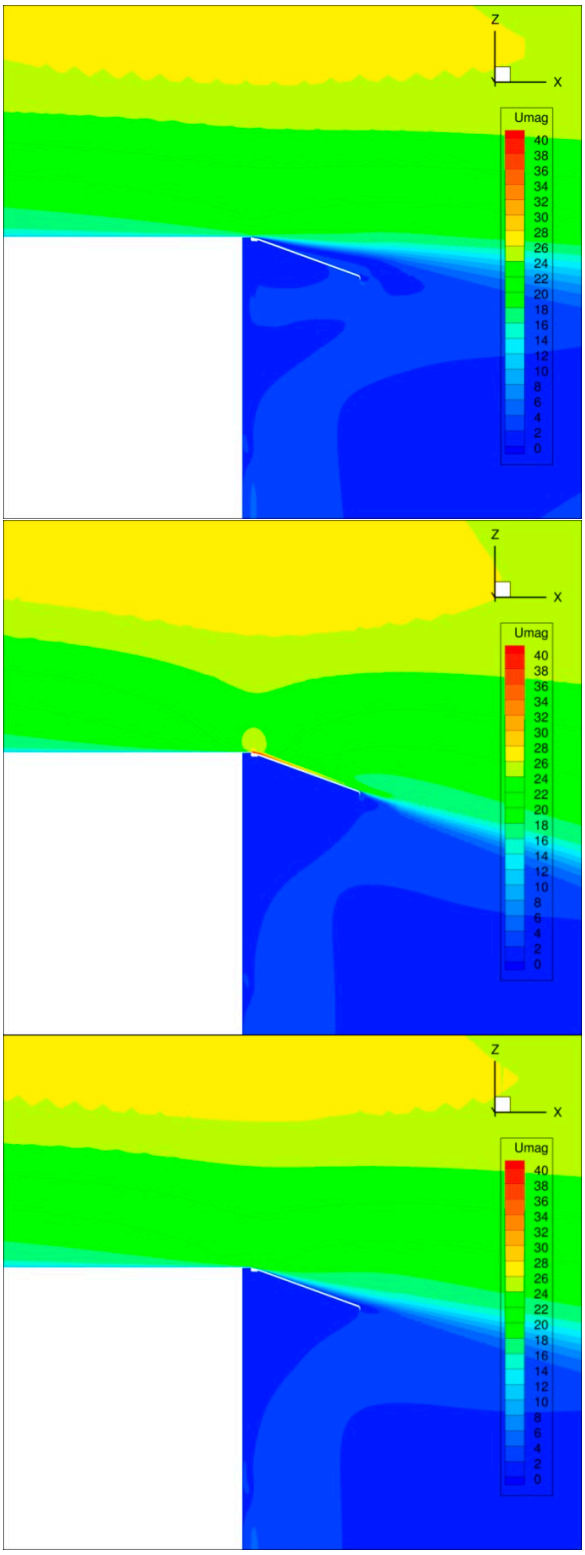

Figure 22: The velocity magnitude in the symmetry plane at 0 degrees sideslip. Top) no tangential blowing, middle) tangential blowing at 60 m/s, bottom) tangential blowing at 25 m/s

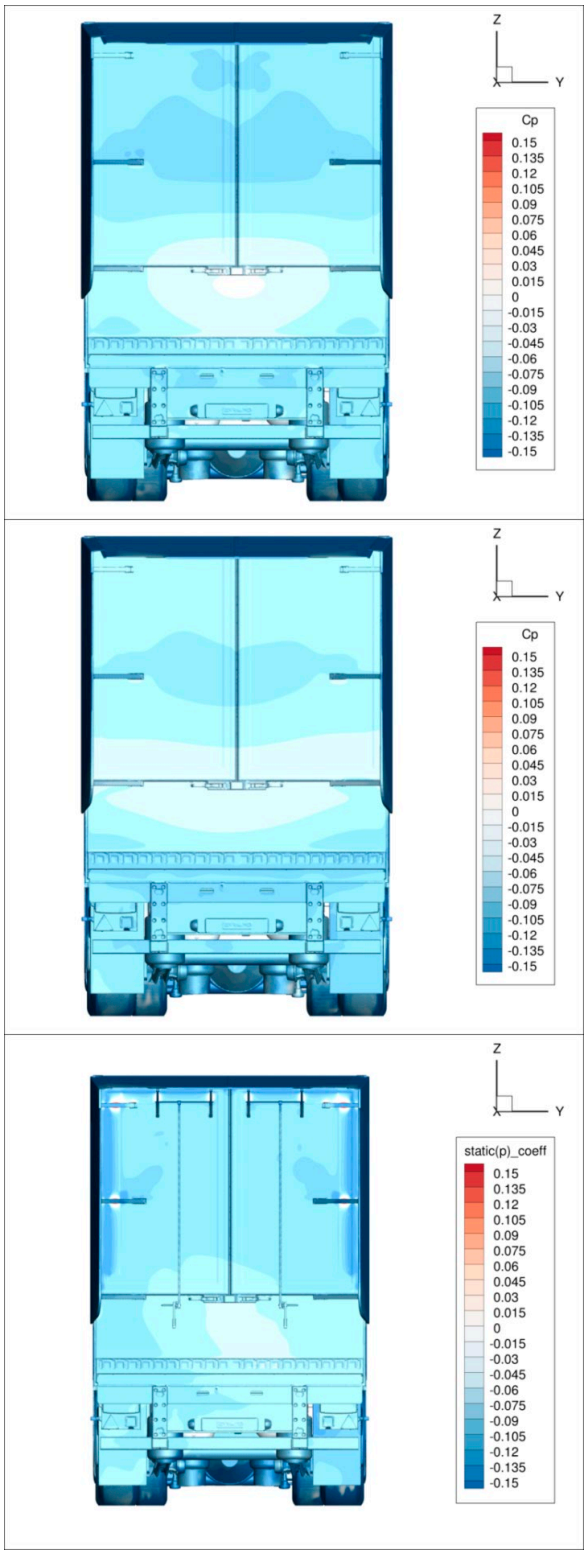

Figure 23: Comparison of the trailer base pressure without blowing (top), with tangential blowing at 60 m/s (middle), with base bleeding at a mass flow rate of 5.5 kg/s

Base bleeding

Base bleeding is implemented as injecting momentum into the wake behind the trailer directly from the base at a low velocity. This is thought to improve the pressure recovery at the trailer base and as such reduce drag. Figure 24 shows the inlet areas for the base bleeding and the lower base bleeding. For the base bleeding, an inlet velocity of 10 m/s was used in combination with a small and large inlet area, leading to two scenarios with a mass flow rate of 3.3 kg/s and 5.5 kg/s respectively. The inlet condition is prescribed such that the flow enters the wake parallel to the boattail panels. Simulations were performed at 0 and -5 degrees of sideslip.

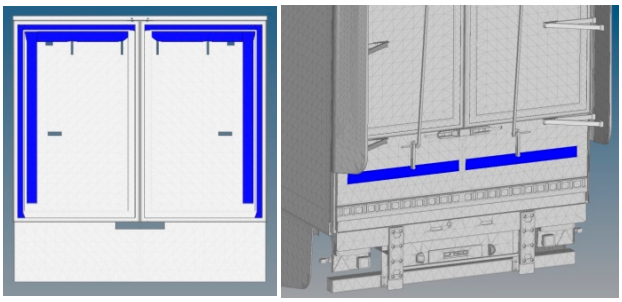

Figure 24: Inlet areas for the base bleeding (left) and lower base bleeding (right) marked in blue

Both intensities of base bleeding lead to a reduction in drag: the mass flow of 3.3 kg/s reduces drag by approximately 2% and the mass flow of 5.5 kg/s reduces drag by 3% to 4%. The higher mass flow leads to a better pressure recovery at the trailer base, see Figure 23. It can also be seen that air that is bled into the wake interacts with the support structures of the boattail, reducing the performance of this method.

Lower base bleeding

Studies have shown that a boattail including the bottom panel has a higher drag reduction potential [6]. Here, this bottom panel is emulated by an air curtain injected into the wake at an upward angle equal to the slant angle of the boattail. Two inlet velocities were used, 25 m/s and 10 m/s at 0 and -5 degrees angle of sideslip.

The wake structure of the baseline geometry and at 25 m/s lower base bleeding is visualized in Figure 25. The baseline wake is dominated by two vortices, with the top vortex rotating clockwise and the bottom vortex rotating counter-clockwise. The wake structure changes when lower base bleeding is applied at a high intensity. The bottom vortex is shifted downward, and the top vortex is pushed away from the trailer base by a new, third vortex closer to the trailer. This new vortex rotates counter-clockwise, and is caused by the lower base bleeding. Its rotation is such that it causes air to move into the airflow coming over the top of the trailer. This has an adverse effect on drag: it is increased by 5% to 6%, see Table 5. Lower base bleeding at a lower velocity does not create this third vortex, and has virtually no impact on the pressure recovery at the trailer base and on the drag.

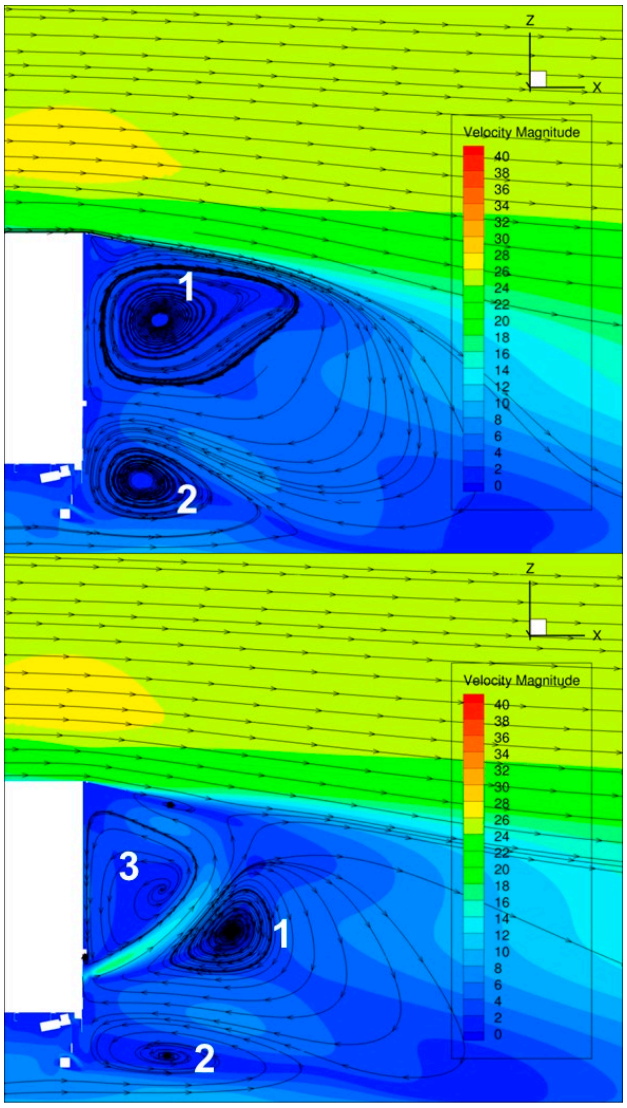

Figure 25: Wake structure of the baseline geometry (top) and with lower base bleeding at an inlet velocity of 25 m/s (bottom)

Conclusions and discussion

An overview of the impact on aerodynamic drag of the discussed concepts is presented in Table 5. The boattail leads to a significant reduction in drag. This conclusion is the same for the GETS configuration including the boattail, although the drag reduction there is much larger, see Table 2. This might be explained by the differences in the geometry of the boattail: the boattail applied to the GETS geometry consists of four panels, where the boattail on the baseline geometry has only three. Furthermore, the baseline and GETS geometry are very different, and differences in drag are therefore to be expected.

Extending the deflectors to cover the truck-trailer gap leads to reduced drag as well. Although fully extending the deflectors seems most effective, extending them partially across this gap still leads to a reduction in drag.

The CFD analyses show that tangential blowing combined with a higher slant angle of the boattail top panel does not lead to a reduction in aerodynamic drag. In this study, the required power to generate the airflow needed for tangential blowing was not considered. If this effect is added to the adverse effect on drag of the higher boattail top panel angle combined with tangential blowing, fuel consumption will likely only increase.

Base bleeding does show a reduction in drag. However, this reduction will have to offset the higher fuel burn required to generate the mass flow needed. If this mass flow could be generated (semi)passively, e.g. by leading air from the trailer top and sides to the low-pressure base, there might be a potential for fuel burn reduction. Compared to the results on the GETS geometry, the drag reduction is lower for the baseline geometry. Mimicking the bottom boattail panel by blowing air into the wake at a high velocity (lower base bleeding) leads to a change in wake structure and an increase in aerodynamic drag.

Table 5: Summary table impact on Cx of selected drag reduction concepts. Values are in drag counts (percentage)

	Angle of sideslip		
Case	**0**	**-5**	**-10**
Baseline geometry	-	-	-
Baseline geometry, boattail removed	33.7 (+11%)	41.6 (+12%)	43.3 (+10%)
Deflecter extension, half	-11.4 (-4%)	-8.3 (-2%)	-15.9 (-4%)
Deflector extension, full	-15.0 (-5%)	-15.4 (-4%)	-24.7 (-6%)
Windward deflector rotation	-	2.5 (+1%)	-13.1 (-3%)
BT top panel 20 degrees, 0 m/s blowing	3.4 (+1%)	7.3 (+2%)	-
BT top panel 20 degrees, 25 m/s blowing	1,7 (+1%)	11.4 (+3%)	-
BT top panel 20 degrees, 60 m/s blowing	3.7 (+1%)	7.1 (+2%)	-
BT top panel 16 degrees, 0 m/s blowing	-2.1 (-1%)	2.7 (+1%)	-
BT top panel 16 degrees, 25 m/s blowing	-2.0 (-1%)	3.3 (+1%)	-
Base bleeding, 3.3 kg/s	-5.7 (-2%)	-5.4 (-2%)	-
Base bleeding, 5.5 kg/s	-12.5 (-4%)	-9.8 (-3%)	-
Lower base bleeding, 25 m/s	14.6 (+5%)	23.3 (+6%)	-
Lower base bleeding, 10 m/s	-3.8 (-1%)	-0.3 (0%)	-

Way forward – verification & validation

Wind tunnel model design/fabrication

NLR has designed and manufactured a high fidelity and modular wind tunnel model of the semi-trailer truck combination (scale 1:3).

The layout of the wind tunnel model consists of a baseline version, corresponding to the geometry shown in Figure 16. Drag reduction concepts can be tested by mounting the concepts to the baseline configuration or by interchanging modular parts of the baseline configuration. This makes it possible to evaluate the effect of one single drag reduction concept as well as a specific combination of drag reduction concepts.

The trailer of the wind tunnel model consists of a load bearing structure made from aluminum struts and an outer shell made from sandwich panels. The outer shell retains the outer geometry of the model as used for the CFD computations. The wind tunnel model is supported by four support arms, connected to the trailer. The four support arms are attached to the balance of the test facility. The tractor is only connected to the trailer and is not supported by any support arms. The truck also consists of a load bearing inner structure with outer shells. The baseline configuration contains a lot of (internal) details which affect the flow, as can be seen from Figure 17. So for CFD validation purposes, the wind tunnel model must contain similar features. Features like fuel tanks, exhaust systems, mud skirts and others are therefore present on the high fidelity wind tunnel model. These features together with the outer shells of the truck are all 3D-printed. An isometric view, showing both the inner structure and outer shells is presented in Figure 26.

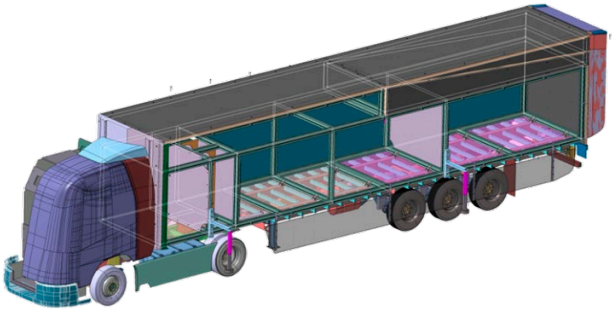

Figure 26: ISO-view of the wind tunnel model

Special attention was paid to the wheels of this wind tunnel model. The trailer wheel subassembly is shown in Figure 27. The complete model can be lowered in the test facility. Lowering the model implies that the vertical distance between the wheels and the underbody of the trailer and truck must decrease. The original air suspension system, present in the baseline geometry files, is included in the model. In the wind tunnel model, the suspension systems functions as a vertical displacement system for the wheels. The vertical distance between the wheels and the underbody of the truck and trailer can be changed with turning buckles. This makes it possible to test variations in ride height. The wheels itself will be driven by the moving belt, which is present in the test facility. This moving belt cannot handle significant vertical loads, therefore the wheels will be positioned such that they touch the moving belt, but the weight is carried by the model. The wheels itself are hollow to reduce weight and balanced to reduce vibrations.

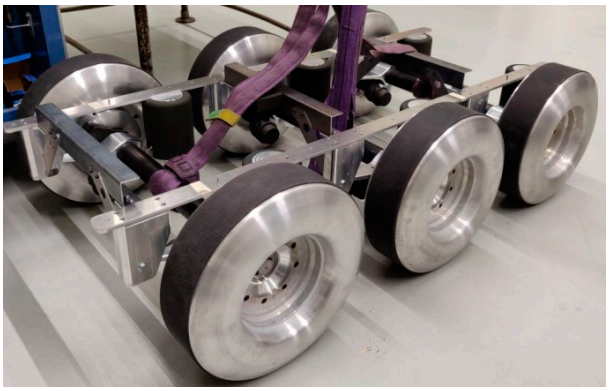

Figure 27: Wheel assembly of the wind tunnel model

In reality the flow can pass through the cooling package and exit the truck by passing around the engine. A simplified engine is 3D printed and installed within the truck to simulate similar internal air flows. The internal flow is simulated by a similar flow channel at the grill. Highly porous metal foam is installed within this flow channel to simulate the pressure drop over the cooling package. The pressure drop over the metal foam can be changed by partially blocking it. In preparation of the test, the pressure drop over the metal foam will be fine-tuned to match the position of the stagnation line between CFD and the wind tunnel test. Minor changes are expected since this metal foam was selected based on measured pressure drop characteristics. The stagnation line will be visualized with the help of tufts.

The wind tunnel model is equipped with 96 static pressure taps. 16 pressure taps are located on the truck and the other 80 are located on the trailer. Most static pressure taps are located on the front and base of the trailer, 20 and 30 respectively. The model is painted matte black to reduce laser reflections during planned PIV measurements.

Wind tunnel experiment set-up and planning

The first wind tunnel test is planned to take place at first week of July 2019 in the Fiat-Chrysler wind tunnel in Turin, Italy. A second wind tunnel entry is scheduled at the end of 2019. The aim of the first wind tunnel entry is to validate CFD computations, while the second entry focusses on combinations of the most promising drag reduction concepts. Additionally, wind tunnel testing of active flow control is planned to mature this technology as drag reduction concept. One active flow control concept will be tested, currently plasma actuators are planned.

To validate CFD, a proper geometrical scale, testing velocity and wind tunnel floor boundary conditions must be realized. The combination of the geometrical scale and planned (maximum) test speed results in a 2/3 full scale Reynolds number. The model will be mounted on a moving belt and the test facility is equipped with a boundary layer suction system just upstream of the moving belt. This makes it possible to simulate a representative boundary layer conditions on the wind tunnel floor (i.e. no boundary layer). The combination of the high fidelity model and the closely matched wind tunnel conditions to full scale conditions, makes it possible to very accurately determine the aerodynamic coefficients and compare it to the high fidelity CFD computations. Uncertainties related to the imperfect matching of the Reynolds number are expected to be small. However, for thorough CFD validation, CFD computations should be performed on wind tunnel Reynolds number.

The wind tunnel test data will contain aerodynamic force and moments, static pressures along the wind tunnel model, boundary layer thickness measurements at several positions on the trailer and flow velocity planes measured with PIV. Results from the wind tunnel campaigns will be presented in a separate publication.

The drag coefficients for the different configurations will be measured at several yaw angles, to determine the wind averaged drag coefficient in accordance with SAE J1252. The wind averaged drag coefficient is the key performance indicator (KPI) for selecting the most promising drag reduction concept.

Acknowledgments

The results in this paper were obtained with partial funding from the European Union's Horizon 2020 research and innovation programme under grant agreement No. 769658, and with partial funding from NLR's Basic Research programme "Kennis voor beleid". The authors would like to thank all partners in Work Package 3 of the AEROFLEX project, i.e. CREO Dynamics, CRF, DAF, IVECO, MAN, SCANIA, Van Eck Trailers, VOLVO, and WABCO, for numerous discussions, feedback and support on CFD activities, wind tunnel model design and manufacture, and test campaign definition.

References

[1] European Commission, "White Paper "Roadmap to a Single European Transport Area - Towards a competitive and resource efficient transport system"," [Online]. Available: https://eur-lex.europa.eu/legal-content/EN/ALL/?uri=CELEX:52011DC0144.

[2] European Environment Agency, "Greenhouse gas emissions from transport," 2018.

[3] "AEROFLEX Project," [Online]. Available: https://aeroflex-project.eu/.

[4] B. Kraaijenhagen, "Aerodynamic and flexible trucks for next generation of," in *International Symposium on Heavy Vehicle Transport Technology*, Rotterdam, 2018.

[5] P. v. Leeuwen, *Masters Thesis: Computational Analysis of Base Drag Reduction Using Active Flow Control,* Delft: Delft University of Technology, 2009.

[6] G. v. Raemdonck, *Design of Low Drag Bluff Road Vehicles,* Delft: Delft University of Technology, 2012.

[7] Siemens, *STAR CCM+ (Version 13.04),* 2018.

[8] *OpenFOAM User Guide,* OpenCFD Limited, 2016.

[9] F. R. Menter, M. Kuntz and R. Langtry, "Ten years of industrial experience with the SST turbulence model," *Turbulence, heat and mass transfer* , vol. 4, no. 1, pp. 625-632, 2003.

[10] A. Bejan, Convection Heat Transfer., John Wiley & Sons, 1984.

[11] J. Ortega and K. Salari, "An Experimental Study of Drag Reduction Devices for a Trailer Underbody and Base," in *34th AIAA Fluid Dynamics Conference and Exhibit*, Portland, 2004.

[12] C. Hakansson and M. J. Lenngren, *CFD Analysis of Aerodynamic Trailer Devices for Drag Reduction (Master Thesis),* Göteborg: Chalmers University of Technology, 2010.

[13] D. G. Hyams, K. Sreenivas, R. Pankajakshan, D. S. Nichols, W. R. Briley and D. L. Whitfield, "Computational simulation of model and full scale Class 8 trucks with drag reduction devices.," *Computers & Fluids,* vol. 41, no. 1, pp. 27-40, 2011.

[14] K. R. Cooper, "Commercial vehicle aerodynamic drag reduction: historical perspective as a guide.," in *The Aerodynamics of Heavy Vehicles: Trucks, Buses, and Trains*, Springer, Berlin, Heidelberg, 2004, pp. 9-28.

[15] H. Chowdhury, H. Moria, A. Ali, I. Khan, F. Alam and S. Watkins, "A study on aerodynamic drag of a semi-trailer truck," *Procedia Engineering,* vol. 56, pp. 201-205, 2013.

[16] S. K. S. B. Ortega J., "Investigation of Tractor Base Bleeding for Heavy Vehicle Aerodynamic Drag Reduction," in *The Aerodynamics of Heavy Vehicles II: Trucks, Buses, and Trains*, Springer, Berlin, Heidelberg, 2009.

[17] B. Storms, D. Satran, J. Heineck and S. Walker, "A Study of Reynolds Number Effects and Drag-Reduction Concepts on a Generic Tractor-Trailer," in *34th AIAA Fluid Dynamics Conference and Exhibit*, Portland, 2004.

[18] R. Wood, "A discussion of a heavy truck advanced aerodynamic trailer system.," in *International Symposium on Heavy Vehicle Weights and Dimensions*, 2006.

[19] R. McCallen, K. Salari, J. Ortega, P. Castellucci, J. Paschkewitz, C. Eastwood, L. Dechant, B. Hassan, W. D. Pointer, F. Browand, C. Radovich, T. Merzel, D. Plocher, A. Leonard, M. Rubel, J. Ross and J. T. Heine, *DOE's Effort to Reduce Truck Aerodynamic Drag Through Joint Experiments and Computations,* SAE International, 2004.

[20] J. Ross, *Heavy vehicle drag reduction experimental evaluation and design.,* 2006.

[21] T. Gustavsson, *Alternative approaches to rear end drag reduction,* Stockholm: KTH, Department of Aeronautical and Vehicle Engineering, 2006.

[22] R. J. Englar, *Development of Pneumatic Aerodynamic Devices to Improve the Performance, Economics, and Safety of Heavy Vehicles,* SAE International, 2000.

[23] M. EL-ALTI, V. CHERNORAY, M. JAHANMIRI and L. DAVIDSON, "EXPERIMENTAL AND COMPUTATIONAL STUDIES OF ACTIVE FLOW CONTROL ON A MODEL TRUCK-TRAILER," in *The European Physical Journal Conferences*, 2011.

[24] A. Seifert, O. Stalnov, D. Sperber, G. Arwatz, V. Palei, S. David, I. Dayan and I. Fono, "Large Trucks Drag Reduction Using Active Flow Control," in *The Aerodynamics of Heavy Vehicles II: Trucks, Buses, and Trains*, 2008.

[25] G. Minelli, E. A. Hartono, L. Hjelm, V. G. Chernoray, B. Basara and S. Krajnovic, *EXPERIMENTAL AND NUMERICAL INVESTIGATION OF ACTIVE FLOW CONTROL ON A GENERIC TRUCK CABIN.,* Chalmers University of Technology, 2016.

[26] M. Varney, M. Passmore and A. Gaylard, *The Effect of Passive Base Ventilation on the Aerodynamic Drag of a Generic SUV vehicle,* SAE International, 2017.

[27] Y. Irving Brown, S. Windsor and A. Gaylard, *The Effect of Base Bleed and Rear Cavities on the Drag of an SUV.,* SAE Technical Papers, 2010.

[28] W. T. Gutierrez, B. Hassan, R. H. Croll and W. H. Rutledge, "Aerodynamics Overview of the Ground Transportation Systems (GTS) Project for Heavy Vehicle Drag Reduction," in *SAE International Congress and Exposition*, Detroit, 1996.

[29] R. Radespiel, M. Burnazzi, M. Casper and P. Scholz, "Active flow control for high lift with steady blowing," *The Aeronautical Journal,* vol. 120, no. 1223, 2016.

[30] G. Minelli, *Drag Reduction by means of Active Flow Control Applied on a Generic Truck A-pillar: a Numerical and Experimental Study,* Götenborg: Chalmers University of Technology, 2016.

Contact Information

The main author can be reached by email via onno.bartels@nlr.nl.

Definitions/Abbreviations

CFVT	Cross-flow vortex trapping
GETS	Generic European Transport System
RANS	Reynolds-averaged Navier-Stokes
SST	Shear stress transport

Dedicated to innovation in aerospace

NLR - Royal Netherlands Aerospace Centre

Royal NLR operates as an unaffiliated research centre, working with its partners towards a better world tomorrow. As part of that, Royal NLR offers innovative solutions and technical expertise, creating a strong competitive position for the commercial sector.

Royal NLR has been a centre of expertise for over a century now, with a deep-seated desire to keep innovating. It is an organisation that works to achieve sustainable, safe, efficient and effective aerospace operations.
The combination of in-depth insights into customers' needs, multidisciplinary expertise and state-of-the-art research facilities makes rapid innovation possible. Both domestically and abroad, Royal NLR plays a pivotal role between science, the commercial sector and governmental authorities, bridging the gap between fundamental research and practical applications. Additionally, Royal NLR is one of the large technological institutes (GTIs) that have been collaborating since 2010 in the Netherlands on applied research as part of the TO2 federation.

From its main offices in Amsterdam and Marknesse plus two satellite offices, Royal NLR helps to create a safe and sustainable society. It works with partners on numerous (defence) programmes, including work on complex composite structures for commercial aircraft and on goal-oriented use of the F-35 fighter. Additionally, Royal NLR helps to achieve both Dutch and European goals and climate objectives in line with the Luchtvaartnota (Aviation Policy Document), the European Green Deal and Flightpath 2050, and by participating in programs such as Clean Sky and SESAR.

For more information visit: **www.nlr.org**

Postal address
PO Box 90502
1006 BM Amsterdam, The Netherlands
e) info@nlr.nl **i)** www.nlr.org

NLR Amsterdam
Anthony Fokkerweg 2
1059 CM Amsterdam, The Netherlands
p) +31 88 511 3113

NLR Marknesse
Voorsterweg 31
8316 PR Marknesse, The Netherlands
p) +31 88 511 4444